


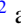




Highly ordered carbon penetration into the $\text{Mn}_5\text{Ge}_3\text{C}_x$ lattice: A superstructure in $\text{Mn}_5\text{Ge}_3\text{C}_{0.5}$ inferred from a ^{55}Mn NMR study

R. Kalvig ¹, E. Jedryka ¹, M. Wojcik ¹, M. Petit ², and L. Michez ²

¹*Institute of Physics, Polish Academy of Sciences, Aleja Lotników 32/46, PL-02668 Warsaw, Poland*

²*Aix Marseille Univ, CNRS, CINAM, Marseille, France*

 (Received 1 June 2021; revised 27 January 2022; accepted 17 February 2022; published 4 March 2022)

Local magnetic properties of the $\text{Mn}_5\text{Ge}_3\text{C}_x(001)$ epitaxial films grown on Ge(111) with a nominal carbon concentration $0 \leq x \leq 0.85$ have been studied by means of ^{55}Mn nuclear magnetic resonance (NMR). The NMR spectra were recorded from the demagnetized films and from the films fully magnetized along the c direction as well as in the hexagonal c plane. The data unambiguously show a synchronized carbon penetration of the crystal lattice ($D8_8$ structure, Nowotny phase, space group $P6_3/mcm$), occupying every second $2(b)$ void located within the chain of $\text{Mn}[6(g)]$ octahedra and setting the limit for the carbon uptake into the Mn_5Ge_3 lattice at $x = 0.5$. Moreover, the NMR data indicate that the chains of carbon-filled voids are correlated also in plane. Eventually, for the end concentration of $x = 0.5$, a highly ordered superstructure is proposed, responsible for the observed two magnetically inequivalent positions within the $\text{Mn}[4(d)]$ sublattice.

DOI: [10.1103/PhysRevB.105.094405](https://doi.org/10.1103/PhysRevB.105.094405)

I. INTRODUCTION

Mn_5Ge_3 thin films, epitaxially grown on Ge(111) substrate, attracted a lot of research interest as a new spintronic material, a potential source of polarized carriers directly into Ge [1]. Mn_5Ge_3 is a metallic ferromagnet with the Curie temperature of 296 K [2,3]. High spin polarization of the conduction electrons at the Fermi level [4] and strong magnetocrystalline anisotropy with an easy axis oriented perpendicular to the film plane [1] open an interesting possibility to combine spintronics with the data storage [5]. Moreover, it has been shown that upon doping with carbon a linear increase of the Curie temperature can be achieved, reaching up to 430 K for the nominal carbon content $x = 0.6$ [where $x = 1$ corresponds to a 100% occupancy of the available $2(b)$ voids in this crystal structure] [1,6].

A spectacular impact of carbon doping on the magnetic properties of Mn_5Ge_3 films calls for a detailed study of the $\text{Mn}_5\text{Ge}_3\text{C}_x$ system using a microscopic method, such as nuclear magnetic resonance (NMR), which provides site-selective information on the local magnetic properties. The use of the NMR experiment in the investigations of magnetic species is due to the fact that the NMR frequency ν probes directly the local magnetic field \vec{B}_{eff} at the site of a studied nucleus. In the previously published paper [7] we have demonstrated that in the absence of external magnetic field the effective field in these materials is practically equal to the hyperfine field \vec{B}_{hf} , the dipolar contribution from the surrounding magnetic moments being one order of magnitude smaller. Therefore,

$$\nu = \gamma |\vec{B}_{\text{eff}}| \simeq \gamma |\vec{B}_{hf}|, \quad (1)$$

where γ is the gyromagnetic ratio. In view of the fact that the dipolar contribution to hyperfine field from the magnetic

moments of $3d$ electrons can also be neglected, as discussed in Ref. [7], the hyperfine field in these materials consists of the contributions from the spin polarization of s electrons due to the s - d exchange interaction with the $3d$ electrons (contact Fermi term \vec{B}_{hf}^{cf}) and from the orbital magnetic moment of $3d$ electrons $\vec{B}_{hf}^{\text{orb}}$ [8],

$$\vec{B}_{hf} = \vec{B}_{hf}^{cf} + \vec{B}_{hf}^{\text{orb}} = A^{cf} \vec{\mu}_s + A^{\text{orb}} \vec{\mu}_{\text{orb}}, \quad (2)$$

where A^{cf} and A^{orb} are the respective hyperfine interaction tensors and $\vec{\mu}_s$, $\vec{\mu}_{\text{orb}}$ denote the spin and orbital magnetic moment of $3d$ electrons. By applying an external magnetic field \vec{B}_{ext} it is possible to differentiate the orbital (anisotropic) and spin (isotropic) contribution to the local magnetic moment $\vec{\mu}_{\text{loc}}$ [7,8]. Moreover, the NMR experiment makes it possible to probe the local atomic environment, since the contact Fermi term \vec{B}_{hf}^{cf} includes the contribution from the on-site magnetic moment as well as from the nearest neighbor magnetic moments.

In our previous papers we have revealed a significant anisotropy of the unquenched orbital moment of manganese in the pristine Mn_5Ge_3 compound, responsible for the bulk uniaxial magnetocrystalline anisotropy [8]. Subsequent NMR studies performed on the diluted C-doped film (composition $\text{Mn}_5\text{Ge}_3\text{C}_{0.2}$ 300 nm thick) have shown that a carbon dopant enters the octahedral $2(b)$ voids in the crystal lattice, lowering the magnetic moment of the six surrounding Mn_{II} [6(g)] atoms by $0.7\mu_B$ and significantly reducing the anisotropy of the orbital moment in those Mn_{II} sites [7]. As a continuation of that study, we present here a systematic ^{55}Mn NMR investigation in the full concentration range of carbon. The outcome of these experiments is rather unexpected: we demonstrate that carbon enters the available lattice voids not randomly, but

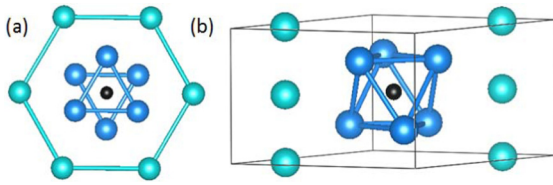


FIG. 1. Atomic arrangement of manganese atoms over two sublattices of $\text{Mn}_5\text{Ge}_3\text{C}$: (a) top view on the hexagonal plane; (b) side view. Colored spheres denote, respectively, Mn_I (green), Mn_{II} (blue), and C dopant (black). This drawing was prepared using the VESTA software [12].

in a highly ordered manner and the highest carbon concentration that the Mn_5Ge_3 lattice can accommodate is $x = 0.5$.

Mn_5Ge_3 crystallizes in the hexagonal $D8_8$ structure (Nowotny phase, space group $P6_3/mcm$) [9,10]. The unit cell contains two formula units. Figure 1 presents the arrangement of manganese atoms, occupying two sublattices: the 4(d) positions (further referred to as the Mn_I sites) and the 6(g) positions (Mn_{II} sites) [9,10]. The octahedron composed of the Mn_{II} atoms forms a $2(b)$ void, which was shown to serve as a host for the carbon dopant [7]. These octahedral “units” create a chain along the c axis, typical for the Nowotny chimney ladder (NCL) compounds.

II. EXPERIMENT

The epitaxial films studied in this paper were grown on a germanium substrate with $\text{Mn}_5\text{Ge}_3(001) \parallel \text{Ge}(111)$ and $[010]$ of $\text{Mn}_5\text{Ge}_3 \parallel [11\bar{2}]$ of Ge; therefore, the hexagonal c plane lies in the plane of the film [11].

The specimens were grown in a molecular beam epitaxy system using solid phase epitaxy (SPE) (see Ref. [13] for experimental details). Reflection high-energy electron diffraction (RHEED) applied *in situ* confirmed a well-developed Ge $c(2 \times 8)$ -reconstructed surface prior to the solid phase reaction. Once the epitaxy was completed, RHEED as well as the *ex situ* x-ray diffraction (XRD) measurements confirmed the formation of a high-quality Mn_5Ge_3 single phase. The C incorporation within the Mn_5Ge_3 lattice barely affects the crystal quality and had no impact on its crystallographic structure [11]. It merely induced perceptible changes in the lattice parameter [11,14] as predicted theoretically [6].

^{55}Mn NMR experiments were performed with the use of an automatic, phase-sensitive spin-echo spectrometer [15]. The spectra have been recorded in the frequency-swept mode, in zero field as well as in the presence of a constant external magnetic field. The ^{55}Mn NMR signals have been collected at 4.2 K in the frequency range 150–500 MHz with the 1 MHz step at several values of the radio frequency field amplitude.

III. RESULTS AND DISCUSSION

Figure 2 presents the ^{55}Mn NMR spectra recorded from a series of 30 nm thick $\text{Mn}_5\text{Ge}_3\text{C}_x$ films with $0 \leq x \leq 0.85$ at zero external magnetic field. In addition, in the top panel we show the NMR spectrum recorded from a 300 nm film with $x = 0$; it consists of two resonance lines corresponding to the two manganese sites in the crystal lattice. Their frequency is

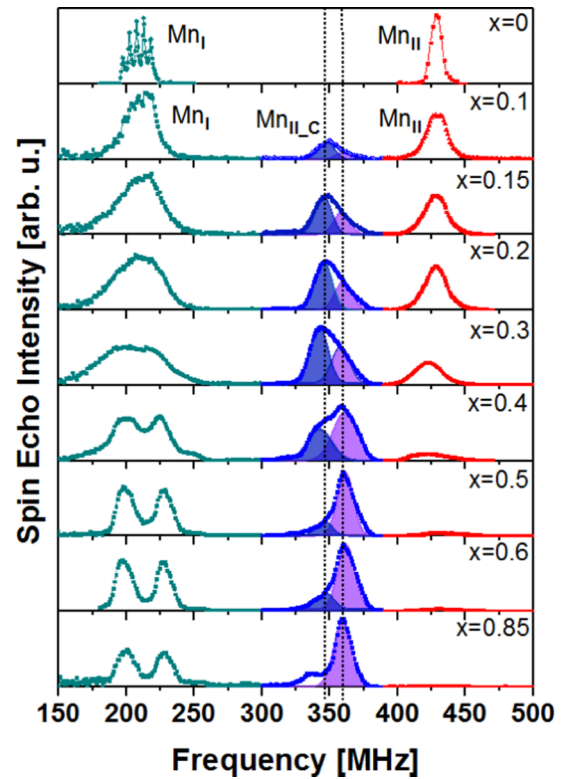


FIG. 2. Zero-field ^{55}Mn NMR spectra recorded at 4.2 K from the 30-nm films of $\text{Mn}_5\text{Ge}_3\text{C}_x$ epitaxially grown on the Ge(111) substrate with a nominal carbon concentration $0 \leq x \leq 0.85$. Green: NMR lines from the Mn_I sites; red: Mn_{II} sites with no carbon nearest neighbors; blue: Mn_{II} sites having carbon nearest neighbors. Top panel: NMR spectrum recorded from the pristine Mn_5Ge_3 epitaxial film 300 nm thick.

centered around 207.5 MHz ($B_{hf} = 19.67T$), further referred to as the Mn_I line, and 428 MHz ($B_{hf} = 40.56T$)—the Mn_{II} line. The large frequency distance reflects the difference in magnetic moment of manganese ($1.94\mu_B$ at the Mn_I site and $3.34\mu_B$ at Mn_{II} [10]). The Mn_I line reveals a characteristic quadrupolar structure due to the fact that the Mn_I site has uniaxial symmetry and a strong electric field gradient (EFG) oriented along the hexagonal c axis (^{55}Mn nuclear spin $I = 5/2$) [8]. A previous NMR study performed on the carbon-diluted ($\text{Mn}_5\text{Ge}_3\text{C}_{0.2}$) 300 nm thick film has shown that the carbon dopant entering the octahedral $2(b)$ voids reduces the magnetic moment of the six surrounding Mn_{II} atoms by $0.7\mu_B$, creating a new subset of the Mn_{II} atoms (further labeled as Mn_{IIc}), that give rise to a new NMR line at 344 MHz [7]. Thin $\text{Mn}_5\text{Ge}_3\text{C}_x$ films investigated in the present study reveal the same NMR lines from three different Mn environments, although the linewidth is broader, compared to the NMR spectrum from a 300 nm sample reported in Ref. [7]. Such broadening is easily understood, considering that the 30 nm thin film is just above the reported thickness limit (28 nm) where the out-of-plane anisotropy prevails over the shape anisotropy [16].

Let us first discuss the carbon-induced evolution of the Mn_{II} line. At low doping levels the NMR line at 428 MHz, characteristic of the unperturbed Mn_{II} environments (red),

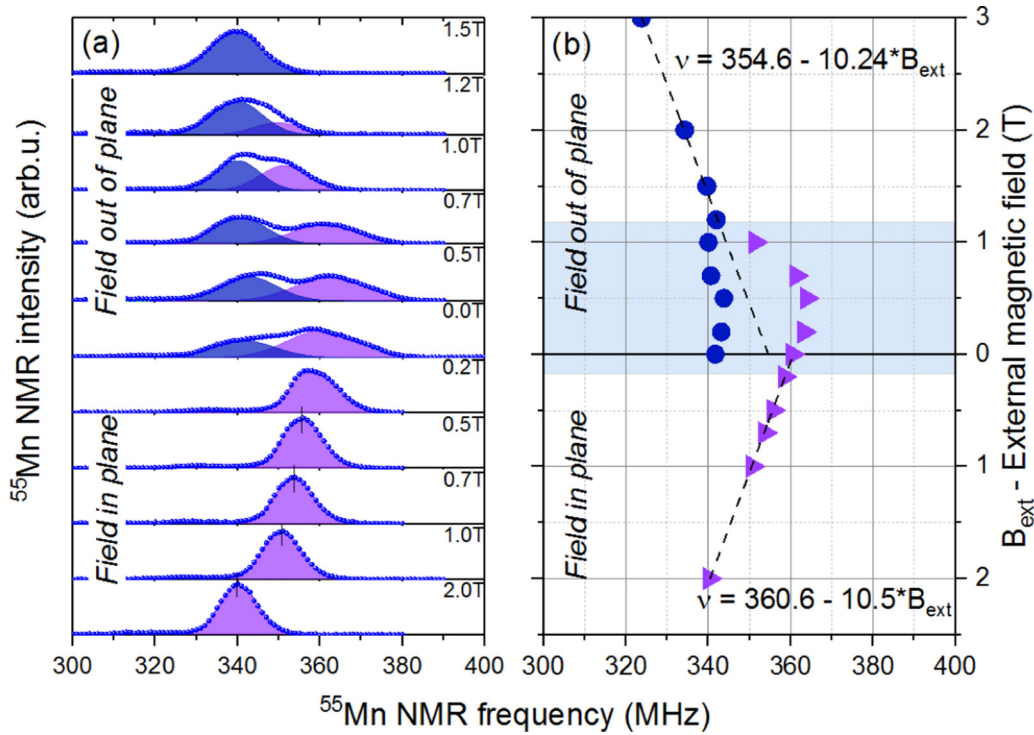


FIG. 3. (a) ^{55}Mn NMR spectra (the Mn_{IIc} line) recorded at 4.2 K from the $\text{Mn}_5\text{Ge}_3\text{C}_{0.4}$ epitaxial film in the presence of the external magnetic field of different values and orientation, as labeled in subsequent panels; (b) central frequency of the two NMR lines shown in (a) as a function of field strength. Purple/blue symbols and shades denote the NMR signals from magnetic moments oriented in-plane/perpendicular to the film plane, respectively. Light blue background denotes the reorientation region.

reveals a rapid drop of intensity with increasing carbon concentration. This rapid drop is due to the fact that every carbon atom entering the octahedral $2(b)$ void affects the six Mn_{II} atoms located in the corners of a host octahedron, reducing their magnetic moment and turning all six of them into the Mn_{IIc} population. At low doping levels this population gives the NMR signal at 344 MHz (blue segment of the NMR spectrum). We note that this line has a tail on the high-frequency side and with increasing carbon concentration a new component, centered around 360 MHz (here marked with a purple filling), comes into the picture, in addition to the original line at 344 MHz. At around $x = 0.4$ this new component becomes a dominant contribution to this part of the NMR spectrum. To find out whether this new component is a result of hyperfine field anisotropy or is a new satellite, a fingerprint of the Mn_{II} environments with two carbon neighbors, we performed experiments in the presence of the external magnetic field applied in plane and out of plane, all the way up to magnetic saturation in the respective direction. Figure 3(a) presents, in the extended frequency scale, the Mn_{IIc} part of the NMR spectra recorded from the $\text{Mn}_5\text{Ge}_3\text{C}_{0.4}$ film at different values and orientation of the external magnetic field.

The zero-field spectrum consists of the two broad overlapping NMR lines centered around 344 MHz and 360 MHz. Upon applying the external magnetic field in the film plane, for the field as low as 0.2 T the spectrum folds down towards the prevailing high-frequency component (purple line in Fig. 3). For the fields stronger than 0.5 T the line shape does not change anymore, whereas the NMR frequency decreases linearly with the slope corresponding to the ^{55}Mn

gyromagnetic ratio (10.553 MHz/T), as shown in Fig. 3(b). The negative slope is to be expected since the external magnetic field acts opposite to the hyperfine field. This experiment unambiguously shows that the component centered around 360 MHz in the zero-field NMR spectrum originates from the magnetic moments oriented in plane. An opposite situation is observed when the external magnetic field is applied in the out-of-plane direction: here the low-frequency component (344 MHz) of the NMR line prevails and its frequency remains constant up to the field of 1.2 T required to fully align the magnetization in the out-of-plane direction. This observation is analogous to that already reported in Ref. [8] and shows that the line at 344 MHz represents the magnetization component oriented along the c axis. The shaded area in Fig. 3(b) denotes the reorientation region where the two spectrum components coexist, but the high-frequency line progressively merges into the low-frequency component, showing that the magnetic moments contributing to this part of the spectrum change their orientation towards the external field direction. The reorientation towards the out-of-plane direction is not as abrupt as it was in the case of in-plane field, where the small portion of the out-of-plane oriented magnetic moments originally giving rise to the 344 MHz line have switched their orientation already at 0.2 T. This is because the shape anisotropy favors the in-plane orientation.

This experiment unambiguously identifies the two components of the zero-field spectra (shown in Fig. 2) as fingerprints of the respective orientations of magnetic moments. In order to shed more light on these observations

we recall that the Mn_5Ge_3 films develop a weak stripe domain structure with broad domain walls and significant presence of closure domains with the in-plane-oriented magnetization [16,17]. In our previous papers [7,8] we have demonstrated that the NMR signal observed in the pristine and weakly doped $\text{Mn}_5\text{Ge}_3\text{C}_x$ films originates predominantly from the magnetization aligned along the hexagonal c direction, which would correspond to the domain wall edge or domain interior. However, the carbon dopant reduces the uniaxial anisotropy, and the contribution from the closure domains with magnetization in the film plane gives a significant contribution to the zero-field NMR spectra, as seen in Fig. 2. At $x \geq 0.5$ the in-plane orientation gives a prevailing contribution to the zero-field NMR spectra. This result not only reflects a significant drop of the uniaxial anisotropy, in agreement with the previous papers [7,16], but—more importantly—it excludes the possibility that the line component centered around 360 MHz could be due to Mn_{II} atoms that happen to have two carbon neighbors, placed in the subsequent $2(b)$ voids, above and below the Mn_{II} atom.

For $x \geq 0.5$ the NMR line from the unperturbed Mn_{II} environments is not observed anymore, showing that every Mn_{II} atom has a carbon neighbor (see Fig. 2). Assuming a statistical distribution of carbon over the $2(b)$ voids, some Mn_{II} sites would have two carbon neighbors and a second satellite line (a new value of hyperfine field) could be expected, which is clearly not the case. Moreover, quite surprisingly, the NMR spectra from the films with a nominal carbon concentration higher than $x = 0.5$ are practically identical. This shows on one hand that $x = 0.5$ is the limit for the carbon intake into the $2(b)$ voids, but it also implies that the distribution of carbon atoms over the $2(b)$ voids is not random and they enter every second available $2(b)$ void in the column created by Mn_{II} octahedra along the hexagonal c direction. Indeed such an ordered fulfillment of every second available octahedron is the only possible configuration leading on one hand to a cutoff carbon concentration at 50% and on the other hand securing that every Mn_{II} atom has a carbon nearest neighbor.

This rather surprising conclusion of the highly ordered void occupancy, is further confirmed by the carbon-induced evolution of the NMR line from the Mn_I atoms (green in Fig. 2). With increasing carbon concentration the Mn_I linewidth increases, smearing the resolution of the quadrupolar structure. Eventually, at around $x = 0.4$ this line bifurcates into two well-resolved components of equal intensity, separated by 29 MHz. However, the origin of this doublet is not the same as the two components of the Mn_{IIc} line, discussed in the previous paragraph, which is proved by the additional NMR experiments in the presence of the external magnetic field strong enough to align all the magnetic moments in the respective direction. Figure 4(b) presents the zero-field ^{55}Mn NMR spectrum (Mn_I line) recorded from the film with $x = 0.5$, whereas in Figs. 4(a) and 4(c) we show the respective spectra recorded in the magnetically saturated state in plane [panel (c)] and out of plane [panel (a)]. The doublet structure persists after magnetic saturation in any direction, showing that it does not originate from the hyperfine field anisotropy. Clearly, it reveals the presence of the two subsets of Mn_I atoms differing in hyperfine fields by 2.75 T, which would correspond to the difference in the on-site magnetic moment of about $0.2\mu_B$.

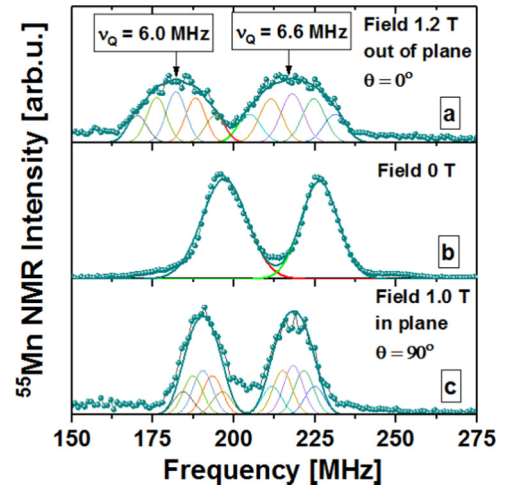


FIG. 4. ^{55}Mn NMR spectra from Mn_I sites in the $\text{Mn}_5\text{Ge}_3\text{C}_{0.5}$ film, featuring two distinct spectrum components. The spectra recorded at 4.2 K from (a) sample magnetically saturated out of plane, (b) demagnetized film, and (c) magnetically saturated in plane. Dotted lines represent the unresolved quadrupolar structure, fitted using $\nu_Q = 6$ MHz and $\nu_Q = 6.6$ MHz, respectively.

Considering that the Mn_I atoms are more distant from the carbon dopant than the Mn_{II} atoms, it is to be expected that the effect of carbon on the Mn_I sublattice is less pronounced.

Although the quadrupolar structure of the Mn_I line is not resolved, the fact that the linewidth of both components of the Mn_I doublet depends on the orientation of magnetization indicates that the quadrupole splitting is the main source of the observed broadening. Consequently, each doublet component can be decomposed into five ($2I$) equidistant NMR lines, as shown in Figs. 4(a) and 4(c). Their frequency separation $\Delta\nu$ is defined by the well-known formula [18]

$$\Delta\nu = (\nu_Q/2)(3 \cos^2\theta - 1), \quad (3)$$

where ν_Q is the quadrupolar frequency—a parameter characterizing the strength of EFG—and θ is the angle between the magnetic moment and the EFG axis. Bearing in mind that the Mn_I site has the uniaxial symmetry along the c axis, $\theta = 0^\circ$ for the out-of-plane direction and—by virtue of Eq. (3)—the quadrupolar splitting is twice as large as in the film plane. This is clearly illustrated in Figs. 4(a) and 4(c), where the NMR spectra from the film magnetically saturated in the respective directions are presented. The linewidth of the zero-field spectrum [Fig. 4(b)] is close to that observed for the film magnetized in plane [Fig. 4(c)], confirming that the NMR signal at carbon concentration $x = 0.5$ originates mainly from the magnetization oriented in plane (as already shown from the analysis of the Mn_{IIc} line). Noteworthy is the fact that the quadrupolar frequency ν_Q is different for each component of the doublet: 6 MHz and 6.6 MHz, respectively. This means that the two subsets of the Mn_I atoms differ not only in the value of the hyperfine field, but also in the EFG strength. Clearly, we observe two distinct Mn_I populations

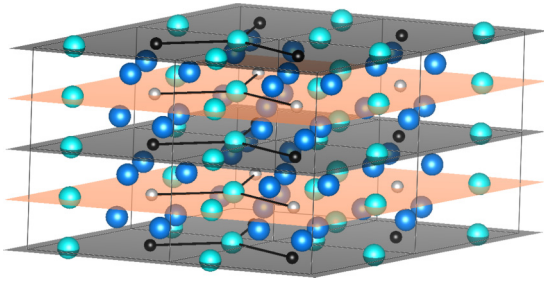


FIG. 5. Schematic representation of a hypothetical carbon superstructure within the $\text{Mn}_5\text{Ge}_3\text{C}_{0.5}$ lattice. Colored spheres denote, respectively, Mn_I (green), Mn_{II} (blue), C (black), and empty $2(b)$ sites (light gray). Two types of the Mn_I planes can be distinguished: gray, all $2(b)$ voids are filled with carbon, and pink, all $2(b)$ voids remain empty.

with slightly different distribution of electric charges around them. Interestingly, none of these populations corresponds to the Mn_I line in the pristine film, where the ν_Q parameter is equal to 5 MHz (cf. top panel in Fig. 1). Bearing in mind that the Mn_I atoms are located in the same atomic planes as the $2(b)$ voids which are the potential hosts for carbon, one can expect that the observed two subsets of Mn_I atoms differ by the number of carbon neighbors.

In short, the following conclusions can be drawn from the NMR experiments: carbon occupies every second $2(b)$ void located within the vertical chain of the $\text{Mn}(6g)$ octahedra along the c axis, thus setting the limit for the carbon uptake into the Mn_5Ge_3 lattice at $x = 0.5$. At carbon concentration of $x = 0.5$ a highly ordered arrangement of the local environments is observed, where the Mn_{II} sublattice is composed of the alternating octahedra (carbon-filled/empty), whereas the Mn_I sublattice has been divided in two, equally populated subsets of atoms that are distinguished by a different number of carbon neighbors in the c plane.

The question now arises of how the vertical chains are oriented with respect to each other, so that they create only two kinds of Mn_I environments existing in the $\text{Mn}_5\text{Ge}_3\text{C}_{0.5}$ lattice. Each Mn_I is surrounded in plane by three $2(b)$ voids. Assuming no synchronization between the neighbor Mn_{II} columns, at $x = 0.5$ one would observe a distribution of different Mn_I environments, with a number of carbon neighbors varying between 0 and 3, and a corresponding broad resonance line, rather than the observed two equally populated resonance lines with the well-defined quadrupolar effect. The most simple arrangement to explain the experimental observations would be a perfect in-plane synchronization: the carbon-containing c planes would alternate with those where the centers of $2(b)$ voids remain empty. Since the Mn_I atoms are located on the same atomic planes as the centers of $2(b)$ voids, half of them would be surrounded by three carbon neighbors, whereas another half of Mn_I atoms would have no carbon neighbor in plane. Such an arrangement constitutes an ideal, highly ordered structure (schematically shown in Fig. 5) and can explain all the features observed in our NMR experiment.

The postulated nanolaminated structure presented in Fig. 5 resembles the MAX phase materials and is likely to host new,

interesting effects. MAX phases are a rich group of compounds described by the general formula $M_{n+1}AX_n$, where M is a transition metal, A stands for an A-group element (mostly group 13 and 14), and X denotes carbon or nitrogen. Recently rediscovered MAX phase compounds display a peculiar combination of ceramic and metallic properties; some of them display complex magnetic behavior [19].

We must stress, however, that nuclear magnetic resonance probes only the local environment; therefore, it cannot be considered as a tool to investigate the long range order. To validate the proposed nanolaminated structure one should consider structural investigations using the diffraction techniques. In particular, neutron diffraction experiment can give reliable information, since the carbon-containing layers would constitute additional scattering planes, differentiating between the carbon-containing planes and those with empty $2(b)$ holes. On the other hand, x-ray diffraction will not be of much use here, due to the weak scattering power of carbon atoms and their small number in the unit cell—the reflex intensity would be very weak, less than 0.3% with respect to the strongest reflex (assuming an ideal long-range order). Nevertheless, to support our conclusion, we note that the parent structure $D8_8$ (Nowotny phase, space group $P6_3/mcm$) seems to be prone to incorporate carbon in a highly ordered manner. Noteworthy is the report on the isostructural $R_5\text{Ge}_3$ materials (R is rare earth), where an ordered $R_{15}\text{Ge}_9\text{C}$ superstructure was observed for $R = \text{Ce}, \text{Pr}, \text{and Nd}$, with the supercell being three times larger than the parent cell [20]. Clearly, the structure described in [20] of the compounds involving rare earth cannot be directly transposed to the Mn-based system studied in this paper. Our data and the data presented in [1] unambiguously show the ongoing modification of the properties and of the local environment beyond 33% of carbon fulfillment of the Mn_5Ge_3 unit cell. Besides, in the ordered $R_{15}\text{Ge}_9\text{C}$ structure there exist still a number of the $R(6g)$ sites in the unperturbed (no carbon neighbors) environment, whereas the superstructure revealed in the present study excludes the presence of pristine $\text{Mn}(6g)$ environments (the original Mn_{II} NMR line is not observed at $x \geq 0.5$). We just point out here that, unlikely as it may seem, a superstructure resulting from the correlated fulfillment of the octahedral voids by carbon has already been observed in the compounds crystallizing in the hexagonal Mn_5Si_3 -type structure (Nowotny phase, space group $P6_3/mcm$).

The comment must also be made regarding the limit of carbon uptake at 50% of the available lattice voids. Some published papers present the results obtained on $\text{Mn}_5\text{Ge}_3\text{C}_x$ films with the nominal stoichiometry higher than $x = 0.5$ [1,21,22]. One possible explanation is that the surplus carbon atoms enter the grain boundaries or lattice imperfections. The observations reported in [1] show, however, a perfect epitaxy up to $x = 0.6$ and a corresponding increase of the Curie temperature. Barring a possibility of a miscalibration, this 10% margin of the carbon atoms may have substituted some germanium atoms. Such a substitution between the nonmagnetic atoms cannot be detected in the NMR experiment. For carbon content higher than $x = 0.6$ the epitaxy was reported to be no longer perfect and cluster formation has been observed, suggesting a possible presence of manganese carbide compounds [1].

IV. CONCLUSIONS

In conclusion, our extensive ^{55}Mn NMR study performed on a series of $\text{Mn}_5\text{Ge}_3\text{C}_x$ ($0 \leq x \leq 0.85$) films with a good epitaxial quality provides strong evidence for a highly correlated carbon penetration into the Mn_5Ge_3 structure, setting the limit for the carbon uptake at $x = 0.5$. A superstructure, consisting in a selective fulfillment of the available lattice voids by carbon, has been postulated for $x = 0.5$, based on the short range order directly observed in the NMR experiments. Such a nanolaminated structure, where

only every second atomic plane hosts carbon atoms, is likely to display new, interesting phenomena, opening the way for further exploration of spintronic effects in this system.

ACKNOWLEDGMENT

We gratefully acknowledge discussions with Prof. P. Dłużewski and Prof. T. Giebultowicz concerning the possibility of validating the proposed superstructure with the x-ray and neutron diffraction spectroscopy.

-
- [1] A. Spiesser, I. Slipukhina, M.-T. Dau, E. Arras, V. Le Thanh, L. A. Michez, P. Pochet, H. Saito, S. Yuasa, M. Jamet, and J. Derrien, *Phys. Rev. B* **84**, 165203 (2011).
 - [2] Ch. Zeng, S. C. Erwin, L. C. Feldman, A. P. Li, R. Jin, Y. Song, J. R. Thompson, and H. H. Weitering, *Appl. Phys. Lett.* **83**, 5002 (2003).
 - [3] A. Spiesser, F. Viro, L. A. Michez, R. Hayn, S. Bertaina, L. Favre, M. Petit, and V. Le Thanh, *Phys. Rev. B* **86**, 035211 (2012).
 - [4] R. P. Panguluri, Ch. Zeng, H. H. Weitering, J. M. Sullivan, S. C. Erwin, and B. Nadgorny, *Phys. Status Solidi B* **242**, R67 (2005).
 - [5] J. M. Shaw, H. T. Nembach, and T. J. Silva, *Phys. Rev. B* **85**, 054412 (2012).
 - [6] I. Slipukhina, E. Arras, Ph. Mavropoulos, and P. Pochet, *Appl. Phys. Lett.* **94**, 192505 (2009).
 - [7] R. Kalvig, E. Jedryka, M. Wojcik, M. Petit, and L. Michez, *Phys. Rev. B* **101**, 094401 (2020).
 - [8] R. Kalvig, E. Jedryka, M. Wojcik, G. Allodi, R. De Renzi, M. Petit, and L. Michez, *Phys. Rev. B* **97**, 174428 (2018).
 - [9] E. Parthé and W. Jeitschko, *Acta Crystallogr.* **19**, 1031 (1965).
 - [10] J. B. Forsyth and P. J. Brown, *J. Phys.: Condens. Matter* **2**, 2713 (1990).
 - [11] M. Petit, L. Michez, Ch. E. Dutoit, S. Bertaina, V. O. Dolocan, V. Heresanu, M. Stoffel, and V. Le Thanh, *Thin Solid Films* **589**, 427 (2015).
 - [12] K. Momma and F. Izumi, *J. Appl. Crystallogr.* **44**, 1272 (2011).
 - [13] S. Olive-Mendez, A. Spiesser, L. A. Michez, V. Le Thanh, A. Glachant, J. Derrien, T. Devillers, A. Barski, and M. Jamet, *Thin Solid Films* **517**, 191 (2008).
 - [14] L. A. Michez, A. Spiesser, M. Petit, S. Bertaina, J. F. Jacquot, D. Dufeu, C. Coudreau, M. Jamet, and V. Le Thanh, *J. Phys.: Condens. Matter* **27**, 266001 (2015).
 - [15] S. Nadolski, M. Wojcik, E. Jedryka, and K. Nesteruk, *J. Magn. Magn. Mater.* **140-144**, 2187 (1995).
 - [16] L. A. Michez, F. Viro, M. Petit, R. Hayn, L. Notin, O. Fruchart, V. Heresanu, M. Jamet, and V. Le Thanh, *J. Appl. Phys.* **118**, 043906 (2015).
 - [17] R. Kalvig, E. Jedryka, P. Aleshkevych, M. Wojcik, W. Bednarski, M. Petit, and L. Michez, *J. Phys. D: Appl. Phys.* **50**, 125001 (2017).
 - [18] A. Abragam, *Principles of Nuclear Magnetism* (Oxford University Press, Oxford, 1961).
 - [19] A. S. Ingason, M. Dahlqvist, and J. Rosen, *J. Phys.: Condens. Matter* **28**, 433003 (2016).
 - [20] F. Wrubl, K. V. Shah, D. A. Joshi, P. Manfrinetti, M. Pani, C. Ritter, and S. K. Dhar, *J. Alloys Compd.* **509**, 6509 (2011).
 - [21] C. Sürgers, G. Fischer, P. Winkel, and H. v. Lohneysen, *Phys. Rev. B* **90**, 104421 (2014).
 - [22] S. Deng, R. Heid, K. P. Bohnen, C. Wang, and C. Sürgers, *Phys. Rev. B* **103**, 134439 (2021).